RSC Advances

ROYAL SOCIETY OF CHEMISTRY

www.rsc.org/advances

Composition dependence of phase structure and electrical properties of $BiMnO_3$-modified $Bi_{0.5}(Na_{0.8}K_{0.2})_{0.5}TiO_3$ thin films

Peng Li[1], Wei Li[1], Jiwei Zhai[1*], Bo Shen[1], Huarong Zeng[2], Kunyu Zhao[2]

1. Key Laboratory of Advanced Civil Engineering Materials of Ministry of Education, Functional Materials Research Laboratory, School of Materials Science & Engineering, Tongji University, Shanghai 201804, China

2. Key Laboratory of Inorganic Functional Materials and Devices, Shanghai Institute of Ceramics, Chinese Academy of Sciences, Shanghai 200050, China

Abstract

In the present study, lead-free (1-x)$Bi_{0.5}(Na_{0.8}K_{0.2})_{0.5}TiO_3$-x$BiMnO_3$ (abbreviated as BNKT-xBMO, with x ranged from 0 to 0.025) thin films were deposited on Pt/Ti/SiO_2/Si substrates by sol-gel method, and the effects of $BiMnO_3$ addition on their crystal structure and electrical properties were systematically investigated. The results show that with increasing $BiMnO_3$ content the crystal structure undergoes the phase transition from a ferroelectric rhombohedral phase to rhombohedral-tetragonal coexisted phases to a relaxor pseudocubic phase. The superior ferroelectric, piezoelectric and dielectric properties were attained at x = 0.01 with remanent polarization $2P_r$ ~14 μC/cm^2, effective piezoelectric coefficient d_{33}^* ~116 pm/V and dielectric constant ε_r ~270. The composition-dependent phase structure and optimal electrical properties indicated that the MPB-like behavior existed at around x = 0.01. Moreover, our study revealed that the end-member $BiMnO_3$ modified BNKT thin films provided a lead-free alternative in ferroelectric

Corresponding author. E-mail address: apzhai@tongji.edu.cn

random access memory (FRAM) and piezoelectric actuators application.

Keywords: BNKT thin film; $BiMnO_3$; Phase structure; Electrical properties

1. Introduction

The development of ferroelectric and piezoelectric thin films started at the late 1960s and early 1970s when great progress in integrated Si devices and thin film processing techniques caused interest in the use of ferroelectric films for fabrication of non-volatile memories, microsensors and actuators.[1-3] At the mid-1980s, the integration of microsensors with microelectronics and the area of micro electro mechanical systems (MEMS) emerged.[2] With the rapid development of thin film preparation technology, piezoelectric thin films based devices are attracting unprecedented attention. Piezoelectric films have been used in a number of commercial products, including piezoelectric microsensors and microactuators due to the good actuating range, a wide frequency range of operation, and a low power consumption. During the past 20 years, the application have triggered intense research toward finding high-performance materials and exploring the relationship between the structure and the properties. The dominant materials for these applications are lead-based systems, such as $Pb(Zr_xTi_{1-x})O_3$ (abbreviated as PZT) because of their superior ferroelectric and piezoelectric properties.[4-7] However, considering the toxicity of lead oxide and demand

for environmentally friendly devices, more and more attention has been paid to the investigation of lead-free composition systems. Currently, extensive studies are focused on $(Bi_{0.5}Na_{0.5})TiO_3$ (BNT) and $(K_{0.5}Na_{0.5})NbO_3$ (KNN) system because of their relatively high piezoelectric and ferroelectric properties.[8-12] For $(Bi_{0.5}Na_{0.5})TiO_3$, it has been expected to be a superior lead-free candidate material because of its good ferroelectricity and relatively high Curie temperature (T_c ~320 ^oC).[13] However, BNT ceramics and thin films have two major drawbacks: (ⅰ) a quite high coercive field, (ⅱ) high conductivity.[14] Compared with pure BNT, many researchers found that BNT-xBKT binary system showed the improved piezoelectric and dielectric properties due to the existent rhombohedral-tetragonal morphotropic phase boundary (MPB).[15-20] Whereas, the investigation of MPB is mainly focused on ceramics, due to the fine grain size and stress in thin films resulting in the MPB is difficult to be obtained.

Up to now, some researches have confirmed that the hybridization between the Pb 6*p* and O 2*p* orbits was responsible for the high piezoelectric response in Pb-based piezoelectric materials. Considering the same electron configuration between Bi^{3+} and Pb^{2+} and bismuth-based perovskite system generally shows high piezoelectric and ferroelectric properties, therefore, more and more attention has been paid to $BiMeO_3$-modified (where Me = Al, Sc, Mn, Fe, etc.) BNT and

KNN-based piezoelectric ceramics.[21-23] Ullah *et al*. have reported that large strain was obtained in $BiAlO_3$-modified $Bi_{0.5}(Na_{0.75}K_{0.25})_{0.5}TiO_3$ piezoelectric ceramics by adjusting the phase structure.[22] In addition, $BiMnO_3$, $BiFeO_3$, $BiScO_3$ with a distorted perovskite-type structure have also been found have evident effects on the structure and electrical properties in BNT-based piezoelectric ceramics.[24-28] However, few studies have focused on the effects of $BiMeO_3$ on the crystal structure and electrical performance of BNT-based thin films. Based on the above consideration, in this work, $BiMnO_3$ was selected as an example to study its effects on the phase structure and electrical properties of BNT-BKT thin films. This work shed light on the potential applications of $BiMnO_3$-modified BNT-BKT thin films for sensors and actuators in MEMS.

2. Experimental

(1-x) $Bi_{0.5}(Na_{0.8}K_{0.2})_{0.5}TiO_3$-x$BiMnO_3$ (x = 0 - 0.025) thin films were prepared by sol-gel method. Sodium acetate [$NaOOCCH_3$] (99%, Alfa Aesar), potassium acetate [CH_3COOK] (99%, Alfa Aesar), bismuth nitrate pentahydrate [$Bi(NO_3)_3 \cdot 5H_2O$] (98%, Alfa Aesar), manganese acetate hydrate [$Mn(CH_3COO)_3 \cdot xH_2O$] (96%, Alfa Aesar), and titanium(Ⅳ) isobutoxide [$Ti(OC_4H_9)_4$] (99+%, Alfa Aesar) were chosen as starting materials and weighted according to the stoichiometric formula. To compensate for the volatility of Na, K, and Bi in the

annealing process, the corresponding material were taken in a 5mol.% excess amount. 2-methoxyethanol and acetic acid were chosen as co-solvent. Acetylacetone [$CH_3COCH_2COCH_3$] was chosen as stabilizer to prevent the hydrolysis of titanium(Ⅳ) isobutoxide. The precursor solution was deposited on Pt/Ti/SiO_2/Si substrates by spin coating at 3000 rpm for 30 s. After each spin-coating the wet thin films were dried at 300 ^oC for 5 min and pyrolyzed at 500 ^oC for 5 min. The spin-coating and heat treatment were repeated for 10 times to obtain the desired thickness. Finally, the thin films were annealed at 700 ^oC for 30 min for crystallization.

The crystal structure of the films was characterized by X-ray diffraction (XRD, D/max-2550V, Rigaku, Japan), operated with Cu Kα radiation. For the electrical measurement, the circular gold top electrodes with radius of 0.5 mm were prepared by DC magnetron sputtering. The polarization hysteresis (*P*-*E*) loops and piezoelectric displacement-voltage (*D*-*V*) loops were measured by a ferroelectric test system (Radiant Precision Premier Ⅱ) and an atomic force microscope (AFM, SPA 400, SPI3800N, Seiko, Japan) equipped with a piezoelectric force mode (PFM), respectively. The electric field dependence of dielectric behavior of these samples were characterized utilizing a precision LCR meter (E4980A Agilent Inc., USA) with a probe station.

3. Results and discussion

Fig. 1 (a) and (b) show the x-ray diffraction (XRD) patterns and fitted peak patterns of BNKT-xBMO thin films, respectively. As can be seen from these patterns, all samples show a pure perovskite phase and no secondary phase could be detected. This result indicates that $BiMnO_3$ has completely diffused into the BNKT lattice to form a new solid solution. In order to determine the phase structure more accurately, the XRD Rietveld refinements were carried out with *R*3*c* space group at room temperature by utilizing the GSAS-EXPGUI program. In view of the needs of the structure refinement, a series of BNKT-xBMO polycrystalline powder samples were prepared by drying and calcining the corresponding gel. In the Rietveld analysis, the refined parameters include background, shift lattice constants, thermal parameters, occupancy, profile half-width parameters (*u*, *v*, *w*), scale factor, atomic functional positions, bond lengths and bond angles. Fig. 1 (c) shows the Rietveld refinement patterns of BNKT-0.02BMO sample as an example, the other samples are similar. The reliability factors, R_{wp} and R_p are 13.92% and 8.96%, respectively, which indicate a good agreement between the refined and experimental data. From the Rietveld refinement results, it can be completely sure that the samples are single perovskite phase. However, the X-ray diffraction patterns indicate that the addition of BMO leads to an obvious change in the phase structure. It can be seen from Fig. 1 (b) that pure BNKT thin films only have a single reflection peak at

2θ around 47°, corresponding to a rhombohedral phase.[16,29] When x = 0.005, the (200) peak shows no apparent splitting, but some degree of broadening peak with left side bulged indicate the phase structure may be change from this composition. However, at x = 0.01 and 0.015, the {200} reflection peak shows significant difference from other compositions, suggesting that there may be two phases in the films. According to peak-fitting results (see Fig. 1 (b)), the {200} reflection splits into two peaks, corresponding to (002) and (200), indicating that the mixed phases of rhombohedral and tetragonal phases exist in these samples.[16,20,24] However, when x > 0.015, the (002)/(200) splitting peaks merge into a single (200) peak, indicating the formation of a pseudocubic phase.[24,30] Similar phase transition has been reported in $BiAlO_3$-modified $Bi_{0.5}(Na_{0.75}K_{0.25})_{0.5}TiO_3$ and $BiScO_3$-modified $Bi_{0.5}(Na_{0.8}K_{0.2})_{0.5}TiO_3$ ceramics.[22,24]

Besides, it is found that with increasing $BiMnO_3$ concentration, the diffraction peaks shift to lower angles, implying the expansion of lattice and increased *d* space. The evolution of lattice can be understood in terms of the ionic radii. It is known that Mn ions prefer to occupy B-site in the perovskite structure. Due to ionic radius of Mn^{3+} (0.65Å) is larger than Ti^{4+} (0.61Å) (refer to Shannon's effective ionic radii),[28] the increase of $BiMnO_3$ contents lead to the expansion of lattice. Consequently, the addition of $BiMnO_3$ induces a distortion in the structural framework and

the phase transition.

Fig. 2 (a) - (c) show the surface morphologies of BNKT-xBMO thin films with various $BiMnO_3$ addition concentration measured by AFM. The surface morphology of the films is granular. The average grain size of the films has been determined by line intercept method as shown in Fig. 2 (d). The error bar of grain size corresponds to the standard deviation of average grain size. It can be seen that the grain size increases sharply with rising BMO content, reaching a maximum value at x = 0.015, implying that a low addition concentration of BMO has entered the lattice of BNKT and promoted the grain growth. Nevertheless, with further increasing BMO content, the grain size reduces dramatically because of the increase of Bi^{3+}, which inhibits the grain growth.[31] Similar phenomena have also been observed in Bi^{3+}-modified KNN ceramics.[32] The physical properties of ferroelectric thin films are closely related to the grain size. Improved remanent polarization, dielectric constant and piezoelectric coefficient were observed with the increase of grain size.[33,34]

Fig. (3) show the ferroelectric hysteresis (*P*-*E*) loops of BNKT-xBMO thin films measured at room temperature with a test frequency of 1 kHz. It can be seen clearly that the *P*-*E* loops strongly depend on the addition concentration of BMO. The remanent polarization P_r values rise with increasing BMO content, reaching a maximum at x = 0.01, and then drop dramatically with x further increasing. The relatively superior

ferroelectric properties obtained in the thin films with x = 0.01 mainly originate from the rhombohedral and tetragonal phases coexistence, which results in the instability of the polarization states and increases the degree of polarization under the external electric field.[31] In addition to phase structure, there are other two factors also contribute to the enhanced ferroelectric properties. On the one hand, the ionic radius of Mn^{3+} is larger than Ti^{4+}, so the B-site Mn^{3+} substitution could enhance the relative ionic displacement and thus increase the dipole polarizability.[18] What's more, as Kan *et al*. reported that the distortion of the B-O octahedra in the perovskite structure can increase the ferroelectricity.[35] On the other hand, domain wall pinning effect will strongly affect the performance in ferroelectric thin films.[18,36] It is well known that the electrons and oxygen vacancies (collectively referred to as charged carrier) will produce in the heat treatment process as described by equation:

$$4Ti^{4+} + 2O^{2-} \rightarrow 4Ti^{3+} + O_2 + 2V_O^{\bullet\bullet} \quad (1)$$

The oxygen vacancies and electrons are easily trapped in the potential well and hinder the domain wall motion. Whereas, the substitution of Mn^{3+} for Ti^{4+} can decrease the oxygen vacancies concentration through forming $\left(Mn_{Ti}^{'} - V_O^{\bullet\bullet} - Mn_{Ti}^{'}\right)$ defect complexes. What's more, Mn ions as an acceptor could prevent the transition between Ti^{4+} and Ti^{3+}, therefore, decrease the electron concentration. Thus the $BiMnO_3$ addition would reduce the carriers and then decrease the pinning of domain wall,

resulting in the improvement of ferroelectric properties. Similar phenomenon has also been reported by Wu and Aksel *et al*. in the Sc^{3+} doped BNKT films and Fe^{3+} doped BNT ceramics, respectively.[18,37] However, when the addition concentration of BMO exceeds 0.015, the remnant polarization begin to decline and the *P*-*E* loops become flat and slender, indicating that the long-range ferroelectric order is disrupted. The pinched *P*-*E* loops can be ascribed to the higher lattice symmetry in the pseudocubic phase, which is consistent with the results in the XRD patterns.

Fig. 4 shows the electric field-induced strain (*D*-*V*) loops and corresponding effective piezoelectric coefficient versus voltage (d_{33}^* - *V*) loops measured at room temperature. The effective piezoelectric coefficient d_{33}^* are obtained according to the slope of every point on the *D* - *V* loops. For all the samples, typical buttefly-shaped electric field-induced strain loops were observed. The nonlinear and hysteretic behavior in these loops indicate that domain wall movement contributes to the strain. The d_{33}^* values of films raise with the increase of BMO content, reaches a maximum (d_{33}^* ~116 pm/V) at x = 0.01, and reduce with further increasing BMO content. The reason why the piezoelectric coefficient d_{33}^* increase with BMO addition can be explained as follows: due to the easy volatility of Bi, Na and K elements in the heat treatment process, the cationic vacancies including Bi, Na and K vacancies can be

formed in the A-site of the perovskite structure. In order to make charge balance the oxygen vacancies will form and be trapped in the grain boundary and the interface between the films and substrates. These cationic and oxygen vacancies could act as pinning center and block the switch of ferroelectric domain. The addition of $BiMnO_3$ would compensate the volatility of Bi and decrease the pinning centers, which promotes the switch of the domains.[18] The larger grain size in BMO-modified BNKT thin films is also beneficial to domain switching. As Xu *et al*. reported that the non-180° domain switching in large grains was much easier and more significant than that in fine grains, which had extrinsic contribution to the piezoelectric response in thin films.[38] On the other hand, the formation of MPB is responsible for the higher piezoelectric properties in the films with x = 0.01 and 0.015. It is well known that the orientation degree of domains is very important to obtain higher piezoelectric properties. In the view of crystallographic, there are 8 domain orientation states in the rhombohedral symmetry perovskite structure because of its spontaneous polarization along <111> direction; there are 6 domain orientation states in the tetragonal symmetry perovskite structure because of its spontaneous polarization along <100> direction. Based on the above results, there are 14 underlying domain orientation states available in these thin films because of the coexistence of the rhombohedral and tetragonal phase, which enhance the probability

of domain switching thus leading to a high piezoelectric properties. The MPB and PPT induced high piezoelectric properties were also reported in BNT-based and KNN-based piezoelectric ceramics and thin films, respectively.[8,20,21,39]

To further analyze the effects of $BiMnO_3$ on the dielectric properties, the dielectric constant ε_r dependent electric field E of thin films were measured under a varying electric field from 0 to 400 kV/cm. As shown in Fig. 4, the characteristic of ε_r - E differ significantly for different BMO addition concentration. When $0 \leq x \leq 0.01$, the ε_r - E loops exhibit evident hysteretic behavior and non-linear dielectric behavior with varying electric field, which indicate ferroelectric domain contributes to the polarization of thin films. However, when $x \geq 0.015$, the samples display indiscernible hysteretic behavior, implying little domain switching. The evident hysteretic behavior and higher tunability at $x = 0.01$ indicate the strong ferroelectric properties in the samples, which is consistent with the results shown in P - E loops. However, at a higher BMO addition concentration ($x > 0.015$), the almost linear and not hysteresis $\varepsilon_r - E$ loops under the applied field indicate that the relaxor phase became dominant due to the prominent reduction in the polarization state, which can also be proved by the slim P - E loops.

Fig. 5 (b) shows the plots of piezoelectric coefficient d_{33}^*, dielectric constant ε_r, and remanent polarization P_r as a function of $BiMnO_3$ content.

It is found that all properties are maximized at the composition near x = 0.01. Generally, MPB is defined as an abrupt structural change and optimal electrical properties with variation in composition.[40] Therefore, it can be concluded that the MPB-like behavior was formed at around x = 0.01. These results are highly consistent with that in $Bi_{0.5}Na_{0.5}TiO_3$–$Bi_{0.5}K_{0.5}TiO_3$–$BiMnO_3$ ceramics.[14] What's more, it is worth noting that the piezoelectric coefficient of 0.99BNKT-0.01BMO thin films is about 116 pm/V. This value is much higher than those of BNT-BKT thin films (d_{33}^* ~70 – 90 pm/V),[20,41] BNT-BT thin films (d_{33}^* ~52 pm/V),[42] and even comparable with PZT thin films (d_{33}^* ~100 – 180 pm/V).[43,44] In the $BiMnO_3$ modified BNKT thin films, the comparable electrical performance with PZT thin films may be related to the lone pair electron in Bi ions. As many studies reported that the hybridization between the Pb 6*p* and O 2*p* orbits is responsible for the large piezoelectric response in Pb-based piezoelectric materials.[21] Taking into account the same electron configuration between Bi ions and Pb ions, Bi^{3+} can hybridize with O^{2-} between the Bi 6*p* and O 2*p* orbits owing to the existence of a lone pair of 6*s* in Bi^{3+}. Therefore, the lone pair electron in Bi ions plays an important role on electrical properties in Bi-containing FE materials.

4. Conclusions

In conclusion, $BiMnO_3$-modified BNKT thin films were successfully

processed on Pt/Ti/SiO_2/Si substrates by sol-gel method. Both phase structure and optimal electrical properties of the thin films demonstrated a strong composition dependence and the MPB-like behavior was found at around x = 0.01 with piezoelectric coefficient d_{33}^* of ~116 pm/V, remanent polarization $2P_r$ of ~14 μC/cm^2, and dielectric constant ε_r of ~270. As a result, this work not only open a window for exploring new material systems but also the $BiMnO_3$-modified $Bi_{0.5}(Na_{0.8}K_{0.2})_{0.5}TiO_3$ thin films are promising candidates for lead-free ferroelectric random access memory (FRAM) and piezoelectric actuator application.

Acknowledgments

This work was supported by the Specialized Research Fund for the Doctoral Program of Higher Education of China (No. 20120072130001), and the National Natural Science Foundation of China under Grant No. 51332003.

References

1 D. W. Chapman, Journal of Applied Physics **40,** 2381 (1969).

2 N. Setter, D. Damjanovic, L. Eng, G. Fox, S. Gevorgian, S. Hong, A. Kingon, H. Kohlstedt, N. Y. Park, G. B. Stephenson, I. Stolitchnov, A. K. Taganstev, D. V. Taylor, T. Yamada, and S. Streiffer, Journal of Applied Physics **100,** 051606 (2006).

3 M. P., Journal of Micromechanics and Microengineering **10,** 136 (2000).

4 S. K. Mishra, D. Pandey, and A. P. Singh, Applied Physics Letters **69,** 1707 (1996).

5 W. Gong, J.-F. Li, X. Chu, Z. Gui, and L. Li, Applied Physics Letters **85,** 3818 (2004).

6 Y. Guo, D. Akai, K. Sawada, and M. Ishida, Solid State Communications **145,** 413 (2008).

7 X. Wan, E. P. Houwman, R. Steenwelle, R. van Schaijk, M. D. Nguyen, M. Dekkers, and G. Rijnders, Applied Physics Letters **104,** 092902 (2014).

8 X. Wang, J. Wu, D. Xiao, J. Zhu, X. Cheng, T. Zheng, B. Zhang, and X. Lou, J Am Chem Soc **136,** 2905 (2014).

9 J. Wu, D. Xiao, and J. Zhu, Chem Rev **115,** 2559 (2015).

10 R. Wang, K. Wang, F. Yao, J.-F. Li, F. H. Schader, K. G. Webber, W. Jo, J. Rödel, and S. Zhang, Journal of the American Ceramic Society**,** n/a (2015).

11 K. Wang, F.-Z. Yao, W. Jo, D. Gobeljic, V. V. Shvartsman, D. C. Lupascu, J.-F. Li, and J. Rödel, Advanced Functional Materials **23,** 4079 (2013).

12 J. Fu, R. Zuo, H. Qi, C. Zhang, J. Li, and L. Li, Applied Physics Letters **105,** 242903 (2014).

13 G. Smolenskii, V. Isupov, A. Agranovskaya, and N. Krainik, Soviet Physics-Solid State **2,** 2651 (1961).

14 HUABIN YANG, XU SHAN, CHANGRONG ZHOU, QIN ZHOU, W. LI，, and J. CHENG，, Bulletin of Materials Science **36,** 265 (2013).

15 W. Bai, J. Xi, J. Zhang, B. Shen, J. Zhai, and H. Yan, Journal of the European Ceramic Society **35,** 2489 (2015).

16 Y.-R. Zhang, J.-F. Li, B.-P. Zhang, and C.-E. Peng, Journal of Applied Physics **103,** 074109 (2008).

17 D. S. Lee, D. H. Lim, M. S. Kim, K. H. Kim, and S. J. Jeong, Applied Physics Letters **99,** 062906 (2011).

18 Y. Wu, X. Wang, and L. Li, Journal of the American Ceramic Society **94,** 2518 (2011).

19 G. Yueqiu, D. Hui, Z. Xuejun, P. Jinfeng, L. Xujun, and H. Renjie, Journal of Physics D: Applied Physics **45,** 305301 (2012).

20 X. J. Zheng, J. Y. Liu, J. F. Peng, X. Liu, Y. Q. Gong, K. S. Zhou, and D. H. Huang, Thin Solid Films **548,** 118 (2013).

21 H. Du, W. Zhou, F. Luo, D. Zhu, S. Qu, Y. Li, and Z. Pei, Journal of Applied

Physics **104,** 034104 (2008).

22 A. Ullah, C. W. Ahn, A. Hussain, S. Y. Lee, and I. W. Kim, Journal of the American Ceramic Society **94,** 3915 (2011).

23 H. Yu and Z.-G. Ye, Applied Physics Letters **93,** 112902 (2008).

24 J. Hao, B. Shen, J. Zhai, H. Chen, and S. Zhang, Journal of the American Ceramic Society **97,** 1776 (2014).

25 C. Zhou, X. Liu, W. Li, and C. Yuan, Materials Chemistry and Physics **114,** 832 (2009).

26 H. Jeen, G. Singh-Bhalla, P. R. Mickel, K. Voigt, C. Morien, S. Tongay, A. F. Hebard, and A. Biswas, Journal of Applied Physics **109,** 074104 (2011).

27 HUABIN YANG, XU SHAN, CHANGRONG ZHOU, QIN ZHOU, WEIZHOU LI, and JUN CHENG, Bulletin of Materials Science **36,** 265 (2013).

28 HUABIN YANG, XU SHAN, C. ZHOU，, QIN ZHOU, W. LI，, and J. CHENG, Bulletin of Materials Science **36,** 265 (2013).

29 C. Peng, J.-F. Li, and W. Gong, Materials Letters **59,** 1576 (2005).

30 I. K. Hong, H. S. Han, C. H. Yoon, H. N. Ji, W. P. Tai, and J. S. Lee, Journal of Intelligent Material Systems and Structures **24,** 1343 (2012).

31 Qian Gou, Ding-Quan Xiao, Bo Wu, Min Xiao, Sha-Sha Feng, Dan-Dan Ma Zhao, Jia-Gang Wu, and J.-G. Zhu, RSC Adv. **5,** 30660 (2015).

32 H. Du, W. Zhou, D. Zhu, L. Fa, S. Qu, Y. Li, and Z. Pei, Journal of the American Ceramic Society **91,** 2903 (2008).

33 W. Li, H. Zeng, J. Hao, and J. Zhai, Journal of Alloys and Compounds **580,** 157 (2013).

34 D. Do, J. W. Kim, and S. S. Kim, Applied Physics A **108,** 357 (2012).

35 E. Kan, H. Xiang, C. Lee, F. Wu, J. Yang, and M. H. Whangbo, Angew Chem Int Ed Engl **49,** 1603 (2010).

36 Y. Noguchi, T. Matsumoto, and M. Miyayama, Japanese Journal of Applied Physics **44,** L570 (2005).

37 E. Aksel, E. Erdem, P. Jakes, J. L. Jones, and R. d.-A. Eichel, Applied Physics

Letters **97,** 012903 (2010).

38 F. Xu, S. Trolier-McKinstry, W. Ren, B. Xu, Z. L. Xie, and K. J. Hemker, Journal of Applied Physics **89,** 1336 (2001).

39 Sun W, Li J F, Yu Q, and C. L. Q, Journal of Materials Chemistry C**,** 2115 (2015).

40 Q. R. Lin, D. Y. Wang, B. C. Luo, R. Ding, D. L. Lorenzen, and S. Li, Applied Surface Science **331,** 477 (2015).

41 Y. H. Jeon, E. A. Patterson, D. P. Cann, P. Mardilovich, W. Stickel, B. J. Gibbons, and S. Zhang, Journal of the American Ceramic Society **96,** 2172 (2013).

42 S. K. Acharya, S.-K. Lee, J.-H. Hyung, Y.-H. Yang, B.-H. Kim, and B.-G. Ahn, Journal of Alloys and Compounds **540,** 204 (2012).

43 W. Gong, J.-F. Li, X. Chu, Z. Gui, and L. Li, Acta Materialia **52,** 2787 (2004).

44 C. Ruangchalermwong, J.-F. Li, Z.-X. Zhu, F. Lai, and S. Muensit, Thin Solid Films **517,** 6599 (2009).

Figure Captions

Fig. 1 (a) X-ray diffraction patterns of BNKT-xBMO thin films at the 2θ range of 20 - 60°; (b) fitted peak patterns of BNKT-xBMO thin films (x = 0, 0.01, 0.015, 0.025) at the 2θ range of 46 - 48°; (c) Rietveld refinement patterns of BNKT-0.02BMO.

Fig. 2 Surface morphology of BNKT-xBMO thin films: (a) x = 0; (b) x = 0.01; (c) x = 0.025; (d) grain size dependence of $BiMnO_3$ addition content.

Fig. 3 Ferroelectric hysteresis (*P* - *E*) loops for the BNKT-xBMO thin films with different BMO addition concentration.

Fig. 4 Field-induced strain (*D*) and effective piezoelectric coefficient (d_{33}^*) versus applied voltage of BNKT-xBMO thin films.

Fig.5 (a) Dielectric constant ε_r dependence of electric field *E*; (b) piezoelectric coefficient d_{33}^*, dielectric constant ε_r and remanent polarization P_r as a function of $BiMnO_3$ addition content.

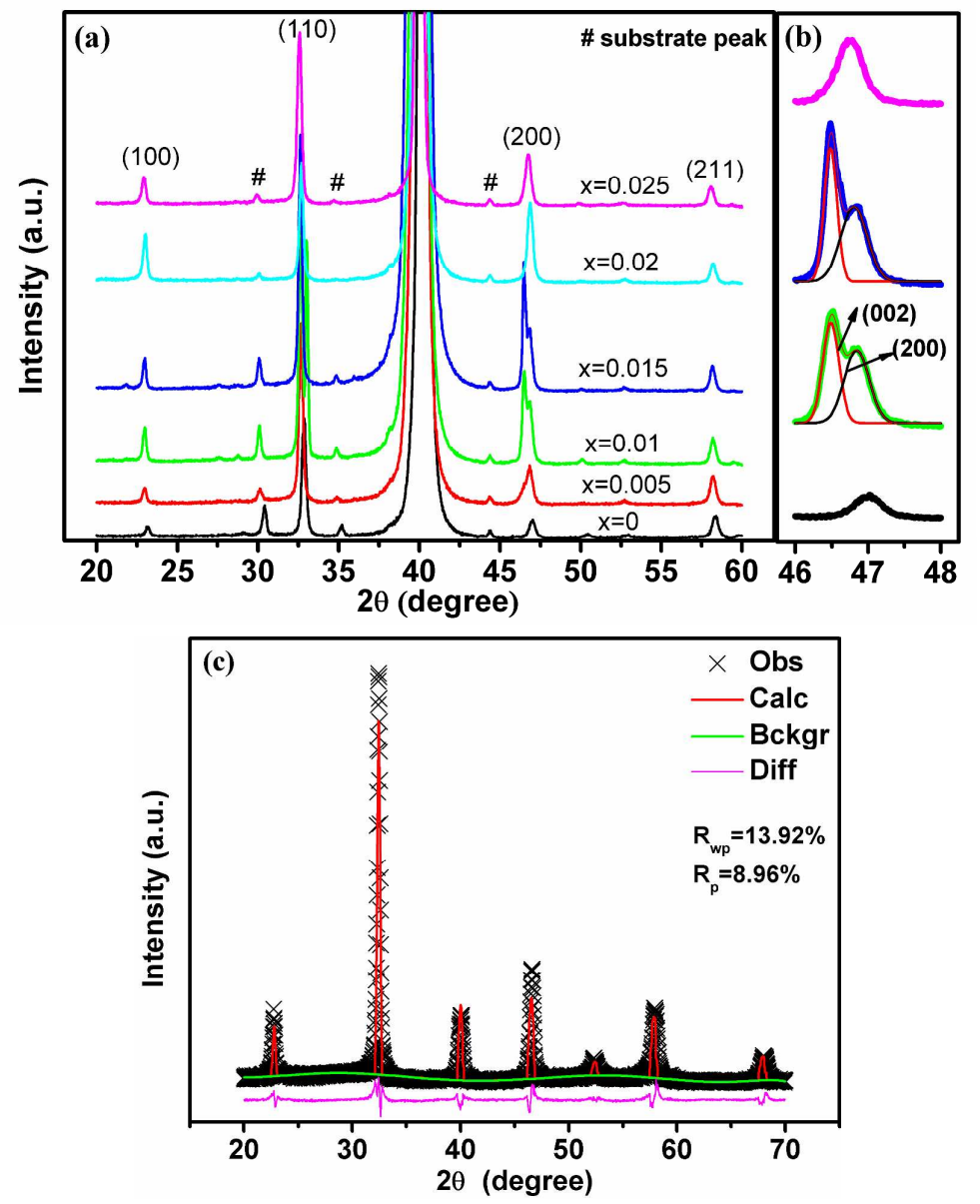

Fig. 1

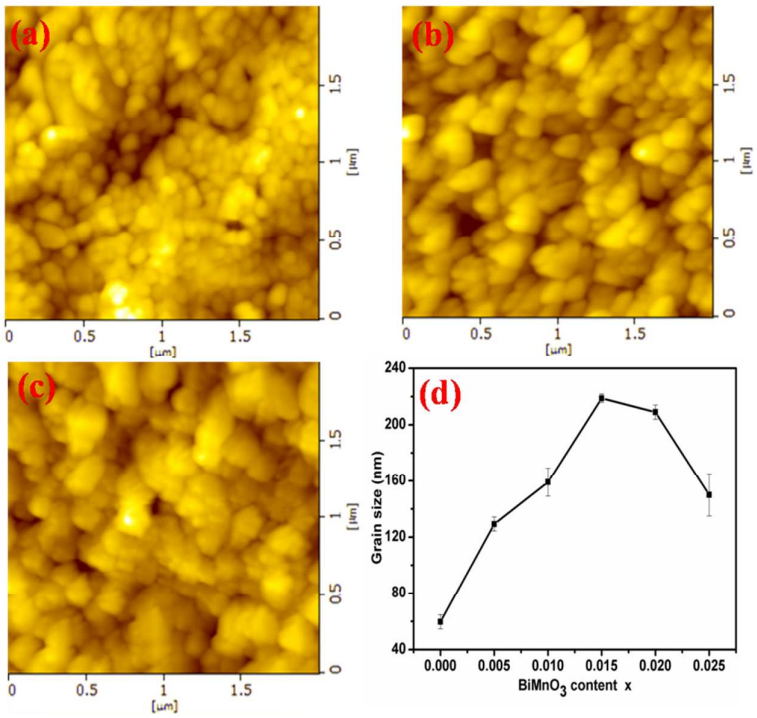

Fig. 2

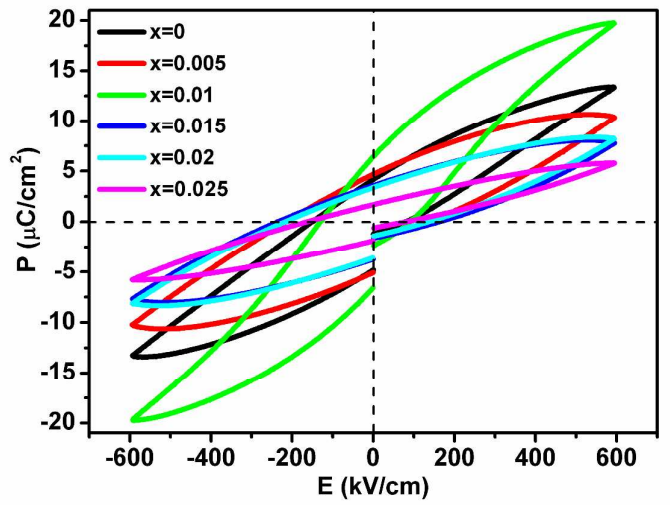

Fig. 3

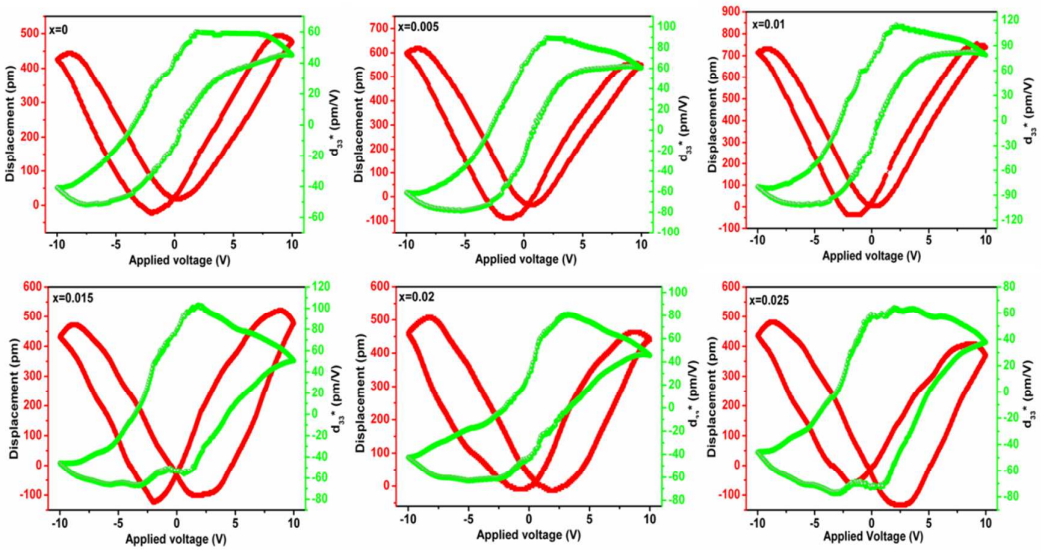

Fig. 4

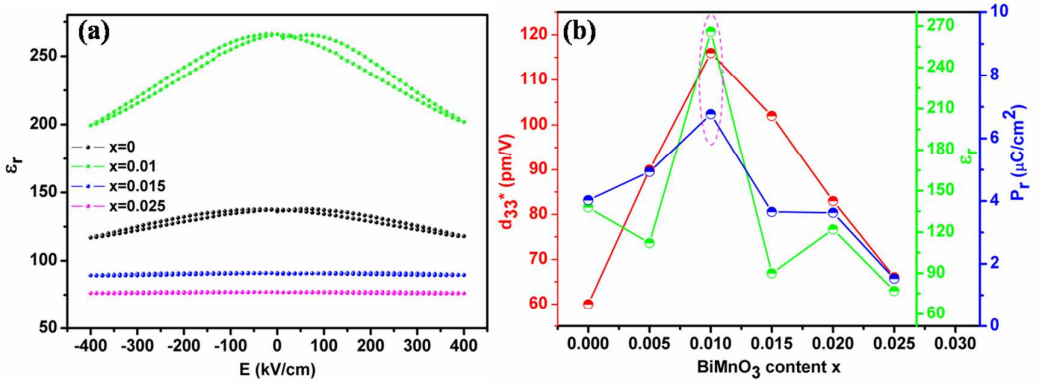

Fig.5